Contribution of sea-ice loss to Arctic amplification is regulated by Pacific Ocean decadal variability

James A. Screen[1] and Jennifer A. Francis[2]

[1]*College of Engineering, Mathematics and Physical Sciences, University of Exeter, Exeter, UK*

[2]*Department of Marine and Coastal Sciences, Rutgers University, New Brunswick, NJ, USA*

The pace of Arctic warming is about double that at lower latitudes – a robust phenomenon known as Arctic amplification (AA)[1]. Many diverse climate processes and feedbacks cause AA[2-7], including positive feedbacks associated with diminished sea ice[6,7]. However, the precise contribution of sea-ice loss to AA remains uncertain[7,8]. Through analyses of both observations and model simulations, we show that the contribution of sea-ice loss to wintertime AA appears dependent on the phase of the Pacific Decadal Oscillation (PDO). Our results suggest that for the same pattern and amount of sea-ice loss, consequent Arctic warming is larger during the negative PDO phase, relative to the positive phase, leading to larger reductions in the poleward gradient of tropospheric thickness and to more pronounced reductions in the upper-level westerlies. Given the oscillatory nature of the PDO, this relationship has the potential to increase skill in decadal-scale predictability of Arctic and sub-Arctic climate. Our results indicate that Arctic warming in response to the ongoing long-term sea-ice decline[9,10] is greater (reduced) during periods of negative (positive) PDO phase. We speculate that the observed recent shift to the positive PDO phase, if maintained and all other factors being equal, could act to temporarily reduce the pace of wintertime Arctic warming in the near-future.

Arctic amplification (AA)[1-8] is a robust feature in observations of the recent past[7,8], paleo-climate reconstructions of the distant past[11], and model projections of the future[12]. The majority of near-surface AA can be explained by feedbacks associated with a diminished sea-ice cover[7,13-15]. Higher in the atmosphere however, the contribution of sea-ice loss to AA is less well constrained[7,8,13-15], in part because the atmosphere response to sea-ice loss appears non-linear and state-dependent[16-19]. By state-dependent we mean that a similar sea-ice anomaly can lead to a different atmospheric response depending on the background ocean-atmospheric state. To date, such state dependencies have generally been attributed to random internal variability[18]. However, known cycles in the ocean-atmosphere coupled system could have a predictable modulating influence on the atmospheric response to sea-ice loss. Here for the first time we present evidence suggesting that the Pacific Decadal Oscillation (PDO) modulates the atmospheric response to sea-ice loss. The PDO is a dominant pattern of sea surface temperature (SST) anomalies that typically persists in predominantly one phase for longer than 10 years (sometimes with temporary reversals to the opposite state) and has wide-ranging effects on global weather and the Pacific ecosystem[20]. The PDO is not a single phenomenon, but is instead the result of a combination of different physical processes[21-23], including stochastic variability of the Aleutian Low, remote tropical forcing and local North Pacific air-sea interactions (see Supplementary Discussion), which can operate on different timescales to drive similar PDO-like SST anomaly patterns[21-23] (Supplementary Figure 1).

The winter PDO index (Fig. 1a) was predominantly negative from winter 1948/49 to 1975/76, mainly positive until winter 2006/07, then negative again in most winters between 2007/08 and 2012/13. In winter 2013/14 the PDO shifted abruptly back to a positive phase and was followed in winter 2014/15 by the most positive PDO value in the 67-year record. Meanwhile, winter Arctic sea-ice area (Fig. 1b) has declined steadily since the late 1970s, one of the most visible indications of human-induced global warming[24-26]. The time-series of the PDO and sea-ice area indices are only weakly correlated (r = -0.25). Although the PDO does not appear to be a strong driver of winter sea-

ice area variability in a pan-Arctic sense, our analysis suggests that the PDO phase affects how the atmosphere responds to sea-ice variability.

Figure 1c,d show composite-mean differences in air temperature between low ice (LI) and high ice (HI) years, respectively, during negative PDO (PDO-) and positive PDO (PDO+). During both PDO phases, negative anomalies in sea-ice area are significantly associated with warmer Arctic air temperatures. The composite anomalies display the classical latitudinal and vertical profile of AA, with greater warming at higher latitudes and at lower altitudes. However, the magnitude of sea-ice-related Arctic warming below 500 hPa is significantly larger during PDO- than during PDO+ (Fig. 1e). At 500 hPa the Arctic-averaged (70-90°N) temperature anomaly is 0.7°C and 0.3°C in PDO- and PDO+, respectively. Corresponding values at 700 hPa are 1.0°C and 0.4°C, and at 850 hPa are 1.2°C and 0.5°C. These results suggest that Arctic warming associated with reduced sea-ice is 75%-150% greater during PDO- compared to PDO+. Larger ice-loss-related Arctic warming is also found during the positive phase of the North Pacific Index (NPI) relative to its negative phase (Supplementary Figure 2), and also to a lesser extent during the negative phase of the El Niño Southern Oscillation (ENSO) relative to its positive phase (Supplementary Figure 3). Compared to the PDO, the NPI more directly measures changes in the Aleutian Low, whereas the ENSO index more directly measures changes in tropical Pacific SST[21-23] (see Supplementary Discussion).

Returning to the PDO influence, it is important to emphasize that the composite sea-ice anomalies are non-identical in the two PDO phases: the difference between LI and HI years is larger for PDO- (Fig. 2a,c), largely owing to the fact that the cases are not evenly distributed in time (the mean year for each case is 1964, 1974, 1996 and 1995 for HI PDO-, HI PDO+, LI PDO- and LI PDO+, respectively). *A priori*, we would expect more warming with larger sea-ice loss. Therefore, a fraction of the observed enhanced warming during PDO- may relate to the larger LI-HI difference in PDO- than in PDO+ (-0.7 million km^2 compared to -0.6 million km^2; i.e., to temporal

inhomogeneity) rather than solely the PDO phase. Assuming that warming scales linearly with sea-ice area loss, we would expect approximately 25% greater warming in PDO- compared to during PDO+. In fact, the observed warming is 75%-150% greater. The additional warming appears to arise from the dependence of sea-ice-induced warming on PDO phase. This hypothesis is difficult to test using observations alone, as statistical association need not imply causation (e.g., interactions between Arctic warming and sea-ice loss are two-way), and other confounding factors cannot be discounted. The results of the observational analysis, however, motivate further study with custom-designed model simulations, which we show provide strong physical support for our hypothesis.

Four atmospheric model experiments were performed (see Methods), prescribed with either an extensive (HI) or reduced (LI) sea-ice cover combined with SST anomalies associated with either PDO+ or PDO-. The differences in prescribed sea-ice concentrations (Fig. 2e) are dominated by reductions in the sub-Arctic seas and along the winter sea-ice edge in the North Atlantic and Baffin Bay. The prescribed PDO-related SST anomalies (Fig. 2f) include warm SST anomalies in the North Pacific and a 'horseshoe' of cool SST anomalies in the central eastern Pacific and along the western coast of North America, typical of PDO-[27] (and also NPI+ and ENSO-; see Supplementary Figure 1). The prescribed anomaly pattern is similar to the observed composite-mean differences in sea-ice and SST (Fig. 2a-d), but with larger magnitude to obtain a more robust simulated response. The atmosphere-only framework has the distinct advantage that sea-ice and SST fields can be perturbed in a controlled way, to isolate their influences on the atmosphere. The major weakness of this approach, however, is that it fails to capture coupled atmosphere-ocean-ice interactions and feedbacks, which may modify the atmospheric response[28].

We now compare the simulations with LI and HI conditions separately for both PDO phases. The four experiments yield two sets of differences (denoted $[\text{LI-HI}]_{\text{PDO-}}$ and $[\text{LI-HI}]_{\text{PDO+}}$), which we subtract ($[\text{LI-HI}]_{\text{PDO-}} - [\text{LI-HI}]_{\text{PDO+}}$), to estimate how the response to sea-ice loss is modulated by

PDO phase. This two-stage process isolates differences in the atmospheric sensitivity to sea-ice loss owing to PDO phase. The zonally-averaged temperature response to sea-ice loss during PDO- (Fig. 3a; $[LI\text{-}HI]_{PDO-}$) displays poleward- and surface-intensified warming. A similar response is simulated during PDO+ (Fig. 3b; $[LI\text{-}HI]_{PDO+}$), but with lesser magnitude over high latitudes. Averaged over the Arctic, the mid-troposphere (500 hPa) warms by 0.4°C and 0.2°C in response to sea-ice loss during PDO- and PDO+, respectively. Analogous values at 700 hPa are 1.4°C and 0.9°C, and at 850 hPa are 3.1°C and 2.4°C. The temperature response difference (Fig. 3c; $[LI\text{-}HI]_{PDO-} - [LI\text{-}HI]_{PDO+}$) more clearly depicts the significantly enhanced Arctic warming below 500 hPa during PDO-. This temperature response difference pattern (Fig. 3c) is in good qualitative agreement with the observed composite difference (Fig. 1e). The consistency between observed and model analyses provides strong support for a causal influence of the PDO phase on the magnitude of sea-ice-induced Arctic atmospheric warming. Furthermore, whilst the interpretation of the *observational* analysis is complicated by the fact that the composites yield unequal sea-ice anomalies (Fig. 2), and by the fact that the PDO-related SST anomalies may be a response to, as well as a driver of, atmospheric variability (see Supplementary Discussion), the *model simulations* unambiguously demonstrate that the Arctic warms more during PDO- compared to PDO+, in response to identical sea-ice loss.

Considering spatial maps rather than zonal means and irrespective of the PDO phase, sea-ice loss induces pan-Arctic warming, with largest magnitudes over the Sea of Okhotsk and west of Greenland (Fig. 4a, shading; $[LI\text{-}HI]_{PDO-,PDO+}$). The enhanced warming response to sea-ice loss during PDO- ($[LI\text{-}HI]_{PDO-} - [LI\text{-}HI]_{PDO+}$) occurs mainly over the central Arctic (Fig. 4b, shading) and north of the regions of winter sea-ice loss (Fig 2e), indicating it is not caused directly by enhanced local surface heat flux changes, which are largely confined (by design) to areas of sea-ice loss. Instead they are caused by advection of warmed (and moistened) air into the central Arctic from the regions of sea-ice loss. To better understand how the PDO phase may influence the

response to sea-ice loss, Fig. 4c (and arrows only in Fig. 4b) presents the direct response to the PDO ($[PDO- - PDO+]_{LI,HI}$). The PDO phase clearly influences the winter-mean atmospheric circulation, principally over the Pacific Ocean (Fig. 4c, arrows), and its influence also extends into the Arctic (Fig. 4b, arrows). Anomalous southerly winds occur during PDO- over the central North Pacific (reflecting a weakened Aleutian Low), which advect air warmed by wintertime sea-ice loss in the Sea of Okhotsk and Bering Sea into the central Arctic. Similarly, anomalous westerly and southerly flow south and east of Greenland during PDO- advects air into the central Arctic that has been warmed by sea-ice loss in the Labrador Sea, Baffin Bay and Greenland Sea. We argue that enhanced ice-loss-driven Arctic warming during PDO-, relative to PDO+, partly arises because the atmospheric circulation during PDO- is more effective at transporting sea-ice-driven temperature anomalies from the peripheral Arctic seas into the central Arctic.

Additionally, aspects of the circulation response to sea-ice loss appear conditional on PDO phase (Fig. 4d, arrows; $[LI-HI]_{PDO-} - [LI-HI]_{PDO+}$), which could be both a driver of and a consequence of the enhanced warming response (Fig. 4d, shading; $[LI-HI]_{PDO-} - [LI-HI]_{PDO+}$). Sea-ice loss causes southerly anomalies in the Beaufort and East Siberian Seas as well as eastward and north of Greenland during PDO-, which further enhance warming in these regions. In short, both the mean circulation during PDO- relative to PDO+ and the sea-ice-driven circulation anomalies during PDO- relative to PDO+ are conducive to warm air advection into the Arctic. This behavior offers a physical explanation for the enhanced Arctic warming response observed both in our model simulations and in the real world.

We emphasize that the enhanced Arctic warming response in PDO- relative to PDO+ is not a direct response to the PDO shift, but rather is an indirect modulation by the PDO of the atmospheric response to sea-ice loss. The PDO has only a weak direct effect on central Arctic temperatures (Fig. 4c, shading) and therefore, the dominant effect of the PDO in the Arctic is indirect through its

influence on wind patterns, which in turn affects the magnitude of Arctic warming owing to sea-ice loss (Fig. 4b, shading).

Returning to the zonally-averaged response to sea-ice loss, we find significantly elevated geopotential heights at high latitudes, increasing in magnitude with altitude, under both PDO phases (Fig. 3d,e; $[LI\text{-}HI]_{PDO-}$, $[LI\text{-}HI]_{PDO+}$). This is a direct response to tropospheric warming dictated by the hypsometric equation. The geopotential height inflation is larger over the Arctic during PDO- relative to PDO+ (Fig. 3f; $[LI\text{-}HI]_{PDO-} - [LI\text{-}HI]_{PDO+}$), consistent with greater high-latitude warming (Fig. 3c). In the 30°N-55°N latitude band, heights decrease significantly, most strongly at upper levels, consistent with a compensating descending motion (Fig. 3c,d). During both PDO phases, sea-ice loss causes weaker westerlies centered near 55°N and stronger westerlies near 35°N (Fig. 3g,h; $[LI\text{-}HI]_{PDO-}$, $[LI\text{-}HI]_{PDO+}$). This response pattern implies an equatorward shift of the mid-latitude storm tracks and associated eddy-driven jetstream, consistent with previous studies of the response to sea-ice loss in atmosphere-only[29] and coupled-model simulations[28]. The wind response is stronger during PDO- compared to PDO+, with further reduced westerlies in latitudes 60°N-75°N throughout the troposphere (Fig. 3i; $[LI\text{-}HI]_{PDO-} - [LI\text{-}HI]_{PDO+}$). These simulations strongly suggest that the greater AA during PDO- versus PDO+ in response to identical sea-ice loss results in a more pronounced reduction in the poleward gradient of geopotential height, leading to larger reductions in the zonal-mean westerlies, with possible implications for mid-latitude weather[5,18,19,30].

In summary, this work is strongly suggestive of an important interaction between natural climate variability and one of the most conspicuous aspects of human-induced climate change: the loss of Arctic sea-ice[24-26]. Our results from both observations and model experiments suggest that AA in response to sea-ice loss is enhanced during PDO-. Given the oscillatory nature of the PDO and other persistent SST patterns (such as that associated with ENSO and NPI; see Supplementary Discussion), improved understanding of such interactions between natural variability and forced

sea-ice change may improve our ability to predict decadal variability and trends in Arctic and sub-Arctic climate. We speculate that the observed recent shift to the positive PDO phase (Fig. 1a), if maintained and all other factors being equal, may act to temporarily reduce the pace of wintertime Arctic warming in the near-future.

References

1. Serreze, M. C. & Barry, R. G. Processes and impacts of Arctic amplification: A research synthesis. *Global and Planetary Change* **77**, 85-96 (2011).
2. Pithan, F. & Mauritsen, T. Arctic amplification dominated by temperature feedbacks in contemporary climate models. *Nature Geoscience* **7**, 181-184 (2014).
3. Bintanja, R., Graversen, R.G. & Hazeleger, W. Arctic winter warming amplified by the thermal inversions and consequent low infrared cooling to space. *Nature Geoscience* **4**, 758-761 (2011).
4. Taylor, P. C., *et al*. A decomposition of feedback contributions to polar warming amplification. *J. Climate* **26**, 7023-7043 (2013).
5. Cohen, J., *et al.* Recent Arctic amplification and extreme mid-latitude weather. *Nature Geoscience* **7**, 627-637 (2014).
6. Burt, M.A., Randall, D.A., & Branson, M.D. Dark warming. *J. Clim.*, **29**, 705-719 (2015).
7. Screen, J. A. & Simmonds, I. The central role of diminishing sea-ice in recent Arctic temperature amplification. *Nature* **464**, 1334-1337 (2010).
8. Graversen, R. G., Mauritsen, T., Tjernström, M., Källén, E. & Svensson, G. Vertical structure of recent Arctic warming. *Nature* **451**, 53–56 (2008).
9. Boe, J., Hall, A., & Qu, X. September sea-ice cover in the Arctic Ocean projected to vanish by 2100. *Nature Geoscience* **2**, 341-343 (2009).
10. Barnhart, K.R, Miller, C.R., Overeem, I. & Kay, J.E. Mapping the future expansion of Arctic open water. *Nature Clim. Change* **6**, 280-285 (2016).

11. Miller, G. H., *et al*. Arctic amplification: can the past constrain the future? *Quaternary Sci. Rev.* **29**, 1779-1790 (2010).
12. Barnes, E. A. & Polvani, L. M. CMIP5 projections of Arctic amplification, of the North American/North Atlantic circulation, and of their relationship. *J. Climate* **28**, 5254-5271 (2015).
13. Screen, J. A., Deser, C. & Simmonds, I. Local and remote controls on observed Arctic warming. *Geophys. Res. Lett.* **39**, L10709 (2012).
14. Perlwitz, J., Hoerling, M. & Dole, R. Arctic tropospheric warming: causes and linkages to lower latitudes. *J. Climate* **28**, 2154-2167 (2015).
15. Kumar, A., *et al*. Contribution of sea ice loss to Arctic amplification. *Geophys. Res. Lett.* **37**, L21701 (2010).
16. Balmaseda, M. A., Ferranti, L., Molteni, F. & Palmer, T. N. Impact of 2007 and 2008 Arctic ice anomalies on the atmospheric circulation: Implications for long-range predictions. *Q. J. R. Meteorol. Soc.* **136**, 1655-1664 (2010).
17. Semenov, V. A. & Latif, M. Nonlinear winter atmospheric circulation response to Arctic sea-ice concentration anomalies for different periods during 1966-2012. *Environ. Res. Lett.* **10**, 054020 (2015).
18. Overland, J., *et al*. The melting Arctic and mid-latitude weather patterns: Are they connected? *J. Climate*, **28**, 7917-7932.
19. Screen, J. A. Arctic amplification decreases temperature variance in northern mid- to high-latitudes. *Nature Climate Change* **4**, 577-582 (2014).
20. Mantua, N. J., Hare, S. R., Zhang, Y., Wallace, J. M. & Francis, R. C. A Pacific interdecadal climate oscillation with impacts on salmon production. *Bull. Amer. Meteorol. Soc.* **78**, 1069-1079 (1997).
21. Newman, M., Compo, G.P. & Alexander, M.A. ENSO-forced variability of the Pacific Decadal Oscillation. *J. Climate* **16**, 3853-3857 (2003).

22. Schneider, N. & Corneulle, B.D. The forcing of the Pacific Decadal Oscillation. *J. Climate* **18**, 4355-4373 (2005).
23. Miller, A.J., Chai, F., Chiba, S., Moisan, J.R. & Neilson, D.J. Decadal-scale climate and ecosystem interactions in the North Pacific Ocean. *J. Oceanography* **60**, 163-188 (2004).
24. IPCC. *Climate Change 2013: The physical science basis*. [Stocker, T. F., Qin, D., Plattner, G. – K., Tignor, M., Allen, S. K., Boschung, J., A. Nauels, Xia, Y., Bex, V. & Midgley, P. M. (eds.)]. Cambridge University Press, Cambridge, United Kingdom and New York, NY, USA, 1535 pp (2013).
25. Notz, D. & Marotzke, J. Observations reveal external driver for Arctic sea-ice retreat. *Geophys. Res. Lett.* **39** L08502 (2012).
26. Min, S.-K., Zhang, X., Zwiers, F.W. & Agnew, T. Human influence on Arctic sea ice detectable from early 1990s onwards. *Geophys. Res. Lett.* **35**, L21701 (2008).
27. Deser, C., Alexander, M. A., Xie, S. –P. & Phillips, A. S. Sea surface temperature variability: patterns and mechanisms. *Ann. Rev. Mar. Sci.* **2010.2**, 115-143 (2010).
28. Deser, C., Tomas, R. A. & Sun, L. The role of ocean-atmosphere coupling in the zonal-mean atmospheric response to Arctic sea-ice loss. *J. Climate* 28, 2168-2186 (2015).
29. Deser, C., Tomas, R. A., Alexander, M. & Lawrence, D. The seasonal atmospheric response to projected Arctic sea-ice loss in the late 21st century. *J. Climate* **23**, 333-351 (2010).
30. Francis, J. A. & Vavrus, S. J. Evidence linking Arctic amplification to extreme weather in mid-latitudes. *Geophys. Res. Lett.* **39**, L06801 (2012).

Correspondence and requests for materials should be addressed to J.A.S.

Acknowledgements. J.A.S. was funded by a UK Natural Environment Research Council (NERC) grants NE/J019585/1 and NE/M006123/1. J.A.F. was supported by an NSF/ARCSS grant (1304097) and NASA grant (NNX14AH896). The model simulations were performed on the

ARCHER UK National Supercomputing Service. We thank the NOAA ESRL and Met Office Hadley Centre for provision of observational and reanalysis data sets. We also thank D. Ackerley for helping to diagnose the cause of model crashes, C. Deser for commenting on the manuscript prior to submission, and two anonymous reviewers for constructive criticism.

Author Contributions. J.A.S. and J.A.F. jointly conceived the study. J.A.S. designed and performed the model experiments, and analyzed the data. Both authors contributed to the interpretation of the results. J.A.S. wrote the manuscript with input from J.A.F**.**

Figures

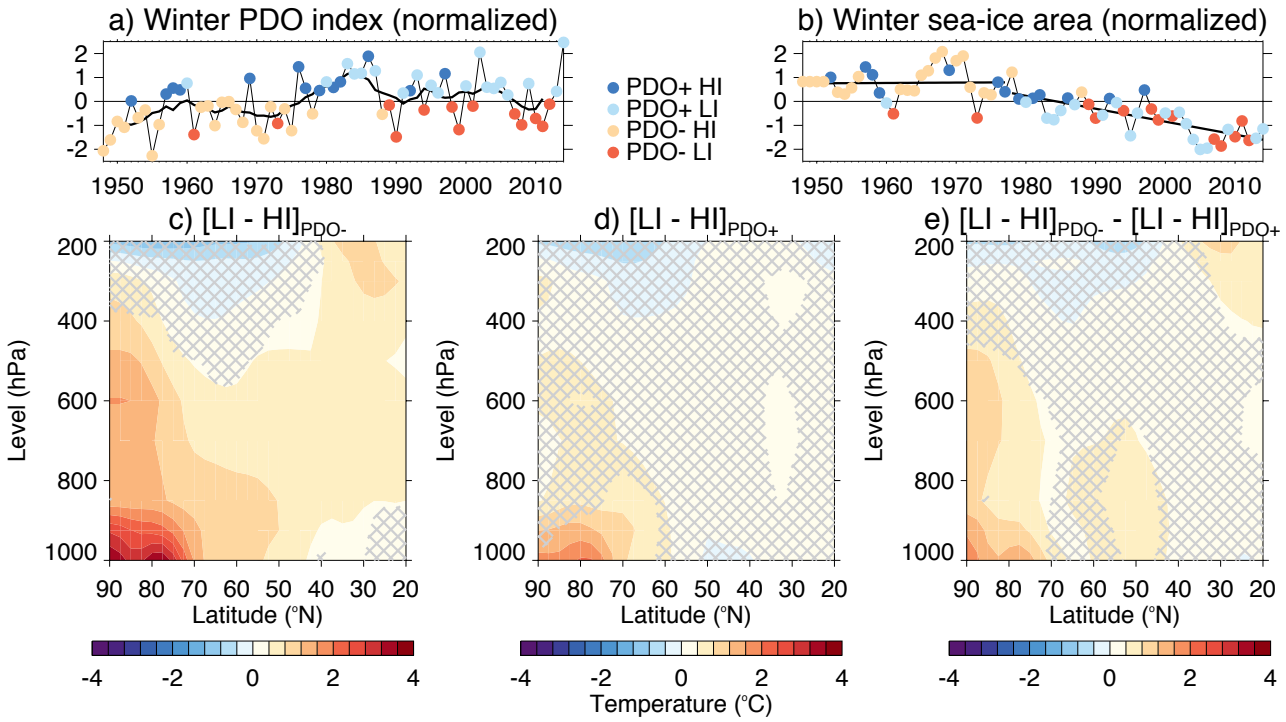

Figure 1: PDO modulation of observed relationship between wintertime Arctic amplification and sea-ice loss. Normalized time series, 1948-2014, of the winter (December-January-February) (**a**) PDO index and (**b**) Arctic sea-ice area. Years on the x-axis correspond to the start of each winter. The years are split into cases when the PDO index was positive or negative and the sea-ice area index was positive (HI) or negative (LI). The thick black line in panel (a) shows the 7-year running mean PDO index, and in panel (b), shows linear trends over two time periods. Composite differences of zonal-mean winter air temperature between years of below-average sea-ice area and above-average sea-ice area during (**c**) PDO- ($[LI-HI]_{PDO-}$) and (**d**) PDO+ ($[LI-HI]_{PDO+}$), and (**e**) their difference ($[LI-HI]_{PDO-}$) - $[LI-HI]_{PDO+}$). Grey hatching denotes composite differences that are not significant at the 95% ($p = 0.05$) confidence level.

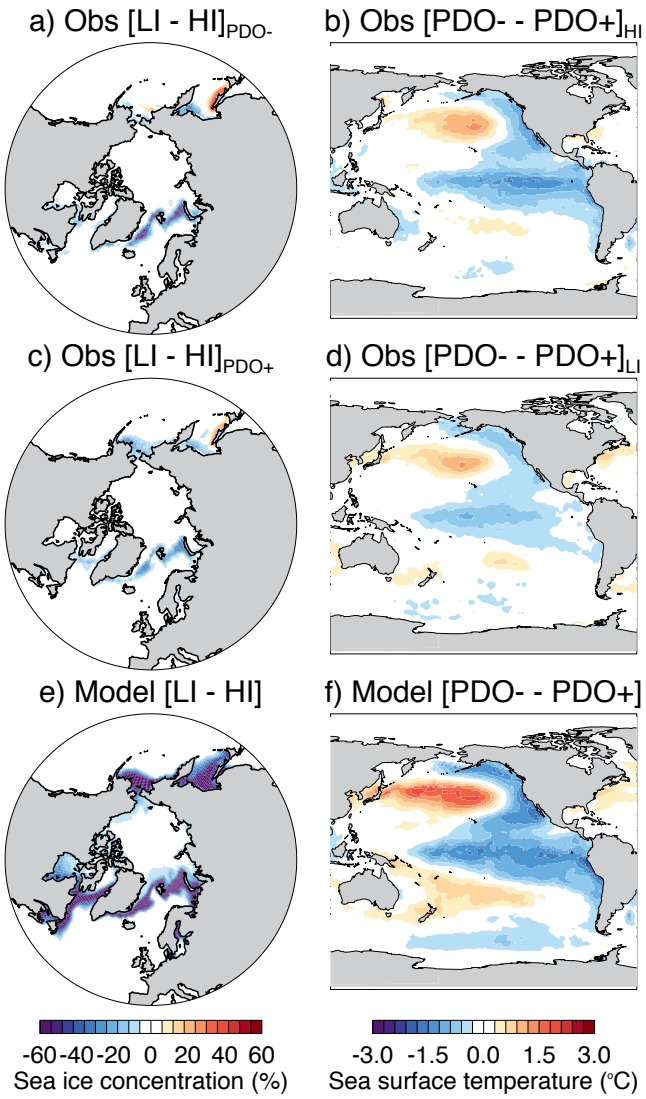

278

279 **Figure 2: Surface signature of wintertime Arctic sea-ice loss and the negative PDO phase.**
280 Composite differences of sea-ice concentration between winters of below-average sea-ice area (LI)
281 and above-average sea-ice area (HI) during (**a**) PDO- ($[LI\text{-}HI]_{PDO-}$) and (**c**) PDO+ ($[LI\text{-}HI]_{PDO+}$).
282 Composite differences of sea surface temperatures between winters of PDO- and PDO+ with (**b**)
283 above-average sea-ice area ($[PDO- - PDO+]_{HI}$) and (**d**) below-average sea-ice area ($[PDO- -$
284 $PDO+]_{LI}$). Prescribed differences in winter (**e**) sea-ice concentrations between the LI and HI
285 experiments, and in (**f**) sea surface temperatures between PDO- and PDO+ experiments.

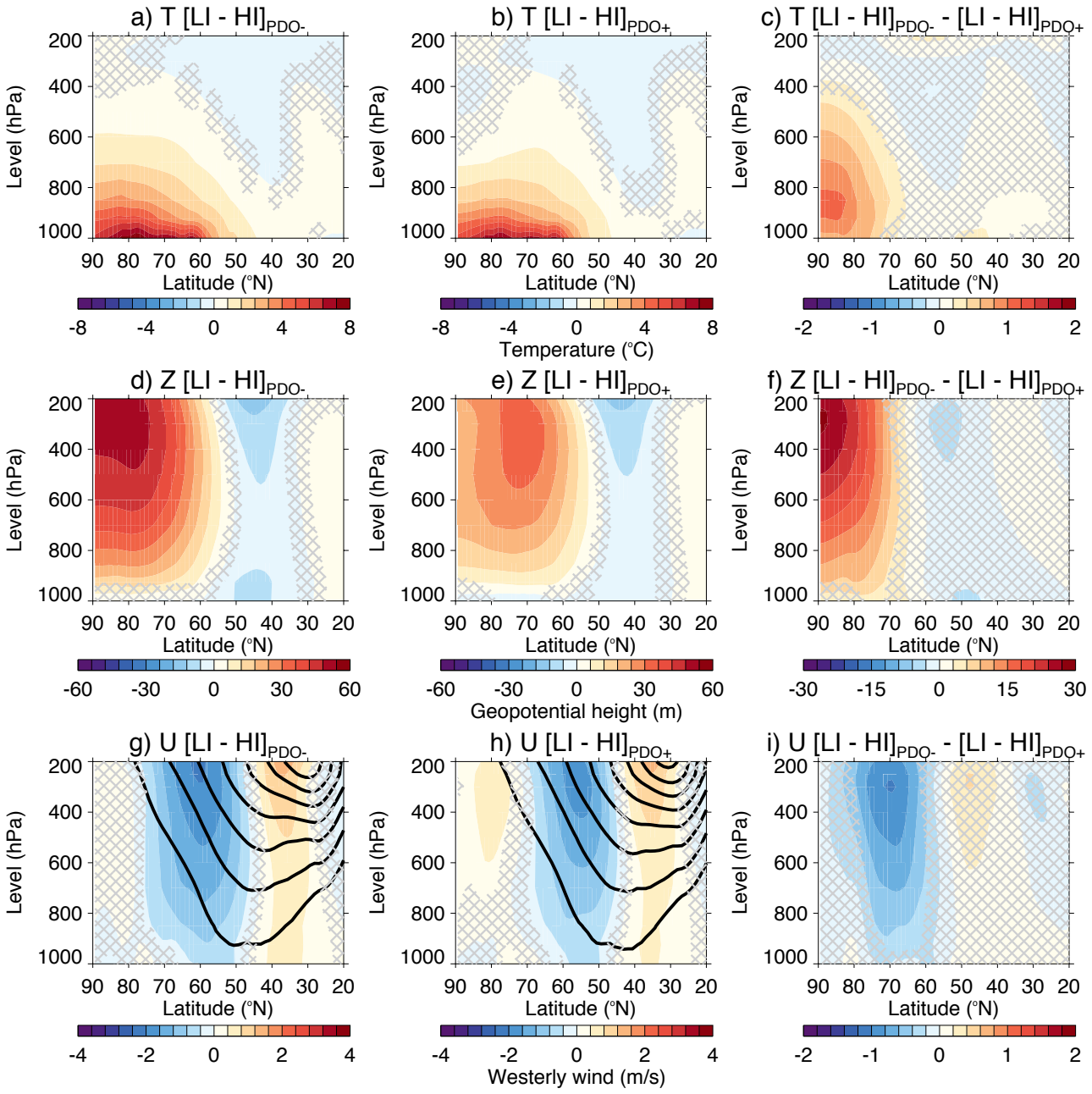

Figure 3: PDO modulation of simulated wintertime atmospheric response to Arctic sea-ice loss. Zonal-mean winter (December-January-February) temperature response to Arctic sea-ice loss during (**a**) PDO- ($[LI-HI]_{PDO-}$) and (**b**) PDO+ ($[LI-HI]_{PDO+}$), and (**c**) their difference ($[LI-HI]_{PDO-}$ - $[LI-HI]_{PDO+}$). As **a-c**, but for (**d-f**) geopotential height and (**g-i**) zonal wind. Grey hatching denotes responses that are not statistically significant at the 95% (p = 0.05) confidence level. Black contours in panels (g) and (h) show the climatological zonal-mean wind (in the HI experiments) and a drawn at intervals of 5 m/s. Note the different color scales in each panel.

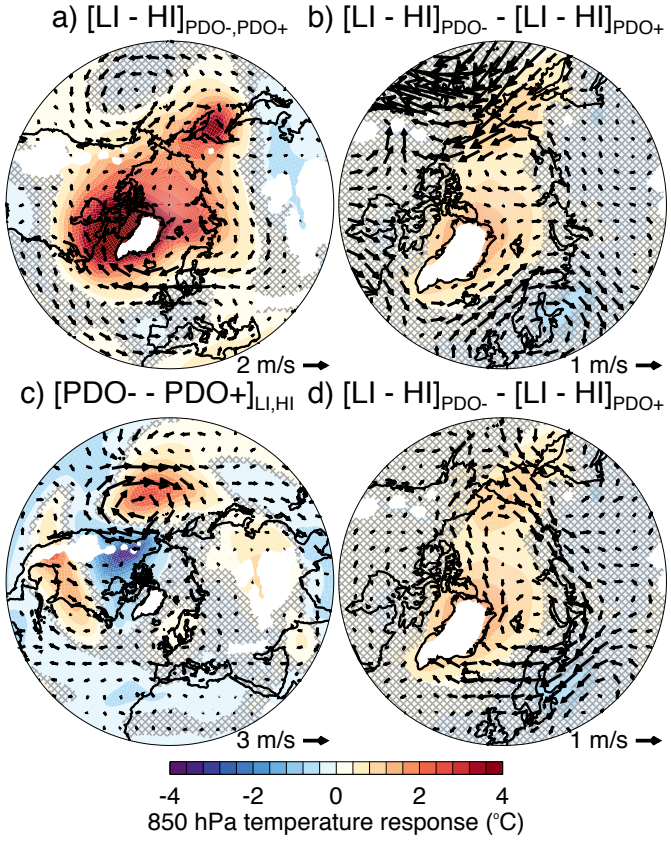

294

295 **Figure 4: Influence of sea-ice loss and the PDO on simulated wintertime lower tropospheric**
296 **temperature and circulation. (a)** 850 hPa temperature (shading) and wind (arrows) responses to
297 Arctic sea-ice loss, independent of the PDO phase ($[LI\text{-}HI]_{PDO\text{-},PDO+}$). (**b**) Differences in 850 hPa
298 temperature (shading) response to Arctic sea-ice loss between PDO- and PDO+ ($[LI\text{-}HI]_{PDO\text{-}}$ - $[LI\text{-}$
299 $HI]_{PDO+}$) overlaid by the 850 hPa wind (arrows) response to PDO- ($[PDO\text{-} - PDO+]_{LI,HI}$). Note the
300 arrows show the direct response to PDO whereas the shading illustrates the indirect modulation of
301 the response to sea-ice loss by the PDO. (**c**) 850 hPa temperature (shading) and wind (arrows)
302 responses to PDO- ($[PDO\text{-} - PDO+]_{LI,HI}$). (**d**) Differences in 850 hPa temperature (shading; repeated
303 from (b)) and wind (arrows; different to (b)) responses to Arctic sea-ice loss between PDO- and
304 PDO+ ($[LI\text{-}HI]_{PDO\text{-}}$ - $[LI\text{-}HI]_{PDO+}$). Grey hatching denotes temperature responses that are not
305 statistically significant at the 95% ($p = 0.05$) confidence level. Regions of elevated topography
306 (where surface pressure falls below 850 hPa) are masked by white shading. Note the different
307 latitudinal lower boundaries and reference wind vectors in each panel.

Methods (Online only)

Data. The PDO, NPI and ENSO indices were obtained from the National Oceanic and Atmospheric Administration (NOAA) Earth System Research Laboratory (ESRL; http://www.esrl.noaa.gov/psd/data/climateindices/list/). Sea ice concentration and SST data are from the UK Met Office Hadley Centre Ice and SST (HadISST)[31] data set (http://www.metoffice.gov.uk/hadobs/hadisst/data/download.html; using the latest version as of May 2015). Global air temperatures are from the National Centers for Environmental Prediction (NCEP) and National Center for Atmospheric Research (NCAR) reanalysis[32] obtained from the NOAA ESRL (http://www.esrl.noaa.gov/psd/data/reanalysis/reanalysis.shtml).

Simulations. Model simulations were performed with the UK Met Office Unified Model[33] version 6.6.3. The model is utilized in an atmosphere-only configuration with prescribed surface boundary conditions. External forcings (e.g., greenhouse gas concentrations, aerosols and so on) are held constant. The model version used here has a horizontal resolution of 1.875° longitude and 1.25° latitude (known as N96) and 38 vertical levels. We performed four ensemble experiments prescribed with either positive or negative sea-ice anomalies in combination with either positive or negative PDO-related SST. These experiments are referred to as *HI/PDO-, LI/PDO-, HI/PDO+* and *LI/PDO+*. Each experiment consists of 150 ensemble members, each 1-year in duration, with the same surface boundary conditions, but starting from a different atmospheric initial condition. The atmosphere-only framework has the distinct advantage that sea-ice and SST fields can be perturbed in a controlled way, to isolate their influences on the atmosphere. The major weakness of this approach, however, is that it fails to capture coupled atmosphere-ocean-ice interactions and feedbacks, which may modify the atmospheric response[28,34]. We analyze simulated variables on atmospheric pressure levels; namely, air temperature, geopotential height, zonal wind and meridional wind. The model data may be made available on request to the lead author.

Surface boundary conditions. For sea-ice, we calculated the monthly-mean climatological mean and standard deviation (σ) of sea-ice concentration, 1979-2013, at each grid-point. For the *HI*

experiments we apply a sea-ice concentration anomaly of +2σ to the climatological mean and for the *LI* experiments we apply an ice concentration anomaly of -2 σ to the climatological mean. At grid-points where a sea-ice anomaly was imposed (i.e., where $\sigma \neq 0$), we also imposed a SST anomaly to account for SST changes linked to sea-ice changes, adapting the approach of ref. 35. For the *HI* experiments we apply a SST anomaly of -2σ to the climatological mean and for the *LI* experiments we apply an SST anomaly of +2σ to the climatological mean. At grid-points where sea-ice is never present or always has the same concentration (i.e., $\sigma = 0$; the latter is the case over the central Arctic where sea-ice concentration is always 100% in winter), the climatological sea-ice concentration and SST was used. Specific ice-related anomalies are applied in each calendar month, but only in the northern hemisphere. To represent the different PDO phases, we first regressed the detrended and normalized annual-mean PDO index, 1948-2013, against detrended annual-mean global SST to yield a SST anomaly per 1σ change in the PDO index (β). For the *PDO+* experiments we apply a SST anomaly of +2β and for the *PDO-* experiments we apply an SST anomaly of -2β. The PDO-related anomalies are applied globally at all ice-free grid-points, with the same PDO-related anomalies (annual-mean) are applied in each calendar month. After applying both the ice- and PDO-related anomalies, we restricted sea-ice concentrations to being between 0-100% and SSTs to no lower than -1.8°C (freezing temperature of saltwater) to avoid unphysical values.

Response estimation. The response to sea-ice loss during PDO- ($[LI\text{-}HI]_{PDO-}$) is estimated by subtracting the ensemble mean (n = 150) in the *HI/PDO-* experiment from that in the *LI/PDO-* experiment. Similarly, the response to sea-ice loss during PDO+ ($[LI\text{-}HI]_{PDO+}$) is estimated by subtracting the ensemble mean (n = 150) in the *HI/PDO+* experiment from that in the *LI/PDO+* experiment. The PDO-dependent component of the response to sea-ice loss is estimated from the difference of the two aforementioned responses ($[LI\text{-}HI]_{PDO-} - [LI\text{-}HI]_{PDO+}$). The PDO-independent response to sea-ice loss ($[LI\text{-}HI]_{PDO+,PDO-}$) is estimated by subtracting the ensemble mean (n = 300) in the concatenated *HI/PDO-* and *HI/PDO+* experiments from that in the concatenated *LI/PDO-* and *LI/PDO+* experiments. The response to the PDO ($[PDO- - PDO+]_{HI,LI}$ is estimated by

360 subtracting the ensemble mean (n = 300) in the concatenated *HI/PDO+* and *LI/PDO+* experiments
361 from that in the concatenated *HI/PDO-* and *LI/PDO-* experiments.
362 **Significance testing.** We compute composite-mean (Fig. 1) and ensemble-mean differences (Fig. 3,
363 4) using a Student's t-test, which compares the sample means to the variances within both samples.
364 The null hypothesis of equal means is rejected with 95% confidence when $p \leq 0.05$.
365
366 **References**

367 31. Rayner, N. A, *et al*. Global analyses of sea surface temperature, sea-ice, and night marine air
368 temperature since the late nineteenth century. *J. Geophys. Res.* **108**, 4407 (2003).
369 32. Kalnay, E. *et al.* The NCEP/NCAR 40-year reanalysis project. *Bull. Amer. Meteor. Soc.* **77**,
370 437-471 (1996).
371 33. Martin, G. M. *et al*. The HadGEM2 family of Met Office Unified Model climate configurations.
372 *Geosci. Model Dev.* **4**, 723-757 (2011).
373 34. Deser, C., Tomas, R.A., Sun, L. & Screen, J.A. Does ocean-coupling matter for the northern
374 extra-tropical response to projected Arctic sea ice loss? *Geophys. Res. Lett.*, in press (2016).
375 35. Screen, J.A., Simmonds, I., Deser, C. & Tomas, R.A. The atmospheric response to three
376 decades of observed Arctic sea-ice loss. *J. Climate* **26**, 1230-1248 (2013).